Analysis of Far-Field Radiation from Apertures Using Monte Carlo Integration Technique

Mohammad Mehdi Fakharian, Pejman Rezaei, and Ali Shahzadi
1- Department of Electrical and Computer Engineering, Semnan University, Semnan, Iran
Email: m_fakharian@sun.semnan.ac.ir

Received: January 2013 Revised: May 2013 Accepted: July 2013

ABSTRACT:
An integration technique based on the use of Monte Carlo Integration (MCI) is proposed for the analysis of the electromagnetic radiation from apertures. The technique that can be applied to the calculation of the aperture antenna radiation patterns is the equivalence principle followed by physical optics, which can then be used to compute far-field antenna radiation patterns. However, this technique is often complex mathematically, because it requires integration over the closed surface. This paper presents an extremely simple formulation to calculate the far-fields from some types of aperture radiators by using MCI technique. The accuracy and effectiveness of this technique are demonstrated in three cases of radiation from the apertures and results are compared with the solutions using FE simulation and Gaussian quadrature rules.

KEYWORDS: Apertures, far-field radiation, Monte Carlo integration, quadrature rule, finite element method.

1. INTRODUCTION

A problem that is often of interest in electromagnetics is the radiation fields out of the aperture antennas, such as slots, open-ended waveguides, horns, reflectors, and lens. The geometry of the aperture may be any shape. Aperture antennas are very popular for aircraft applications because they can be flush mounted onto the surface and the aperture opening can be covered with a radome to protect the antenna from the environmental conditions [1]. This is implemented to maintain the aerodynamic profile of the high-speed aircraft.

In order to evaluate the far-field radiation patterns, it is necessary to know the surface currents on the radiating surfaces of the antenna. Field equivalence [2] is a principle by which the actual sources on an antenna aperture can he replaced by the equivalent sources on an external closed surface outside of the antenna aperture. The fictitious sources are equivalent within a region if they produce the same fields within that region. Huygen's principle [3] states that each point on a primary wave front can be considered to be a new source of a secondary spherical wave and that a secondary wave front can be constructed as the envelope of these secondary spherical waves.

Using these concepts, the electrical and magnetic fields in the equivalent aperture region are determined, and the fields are assumed to be zero elsewhere. In the most applications the closed surface is selected so that the most of it coincides with the conducting parts of the physical antenna aperture structure. This is preferred because vanishing the tangential electrical components over the conducting parts of the surface reduces the limits of the integration.

This is often circumvented by using the equivalence principle to determine the far field by equivalent currents generated in the near field. However, these transformations are often complex mathematically. The Gaussian quadrature rules are used to evaluate the radiation integrals which provide the appropriate weights and evaluation points for the integration [4]. Moreover, many numerical full-wave methods have been proposed for the solution of the electromagnetic radiation from apertures. There are three primary full-wave methods used in the electromagnetics; the Finite Element Method (FEM) [5], [6], the Method of Moments (MOM) [7], and the Finite Difference Time Domain (FDTD) method [8]. All three techniques have been applied to aperture antenna analysis [9]-[12]. This paper presents an extremely simple method for calculating the fields from some types of the aperture radiators. It is proposed to introduce a new fast and efficient algorithm to perform the numerical integration by Monte Carlo Integration (MCI) technique [13]. The MCI technique proposed in this paper is not only capable of solving the radiation problem but also deals efficiently with the problem of singularity.

The application of MCIs in the electromagnetic radiation and scattering problems has been limited to evaluate the statistical average of the physical

quantities over randomly oriented bodies. In [14], the bi static radar scattering cross section of randomly oriented wires has been determined using the MCI methods, whereas the averaging fields in dense random media with dielectric spheroids with random positions and orientations have been evaluated in [15]. A Monte Carlo simulation is used for the problem of the electromagnetic scattering by a collection of random distributed vertical cylinders over a half-space dielectric in [16]. The use of MCI methods to integrate the functions in the moment of the method solution of the electric field integral equation formulation of the scattering problems has been reported in [17], [18]. However, the use of MCI for determining the far-field radiation pattern from an aperture in a metal plate has not been presented so far.

In this paper, the MCI technique has been proposed to solve the radiation integrals for the rectangular, circular, and elliptical apertures. The field distributions over the apertures are considered as the uniform and $TE_{10}/TE_{11}/TE_{c11}$-modes on an infinite ground plane. The radiated field is obtained by the integration of the currents on all the surfaces in much the same way as it is obtained in the physical optics approaches. The numerical simulation based on the FEM for radiation of the aperture antennas is also presented and compared with available data. A good agreement in the comparison confirms the applicability of the method developed in this paper.

2. MATHEMATICAL CONCEPT OF THE MCI TECHNIQUE

Monte Carlo integration is a mathematical technique that relies on the statistical properties of the random variables and sampling to numerically estimate the integrals. It is well suited for the high-dimensional integrals arise from the light transport problem. While standard numerical integration techniques do not work very well on the high-dimensional domains, especially when the integrand is not smooth.

The MCI methods have advantages over the other numerical integration methods, because of:

- The simplicity: The MCI is simple since only two basic operations are required, namely sampling and point evaluation.
- The independence of the dimension: Their efficiencies relative to the other methods increase when the dimension of the problem increases e.g. the quadrature formula becomes very complex while the MCI technique remains almost unchanged in more than one dimension [17], [18].
- The possibility of the integration on the bad shapes and volumes: It is also suited for the large structures and highly complex problems for which definite integral formulation is not obvious and standard analytical techniques are ineffective [17], [18].
- The troubleshooter for the singularity points: Sampling can be used even on the domains that are not well-suited to the numerical quadrature [18].

The idea of the MCI is to evaluate the integral using the random sampling as:

$$I = \int_{\Omega} f(x)dx \tag{1}$$

Where f is a function of vector $\boldsymbol{x}$, Ω is the domain of integration. The MCI is popular for complex f and/or Ω. In its basic form, this is done by independently sampling N points $x_1, \ldots, x_N$ according to some convenient density function p, and then computing the estimate:

$$F_N = \frac{\Omega}{N}\sum_{i=1}^{N}\frac{f(x_i)}{p(x_i)} \tag{2}$$

Where $p(x_i)$ is the probability density function or *pdf*. Here the notation F_N is used rather than I to emphasize that the result is approximate, and that its properties depend on how many sample points are chosen. If $p(x_i)$ is the uniform probability density, then the integral is simply

$$I \cong \frac{\Omega}{N}\sum_{i=1}^{N} f(x_i) \tag{3}$$

In terms of handling the singularity problem in the integrand, the MCI technique outperforms many of the existing techniques. It handles this problem very easily, effectively and efficiently even in situations where there is no analytical transformation available to remove the singularity without changing the form of the kernel of the integrand. There is also no need for any analytical preprocessing or employing any corrective technique. The singularity problem can be handled very efficiently by just preventing the randomly generated points falling in the neighborhood of the singular point [19], [20]. The singular domain can be marked as a small circular region about the point of singularity in two dimensional problems. Exclusion of the singular domain is a straight-forward matter, and can often be performed with one MATLAB code statement.

3. FORMULATION OF THE RADIATION FIELDS FROM APERTURES

The particular configuration we are concerned with in this paper is an aperture in an infinite metal plate, as illustrated in Fig. 1. We assume that there is a source impinging from the bottom (negative Z axis), which is primarily polarized in the X direction, and we are interested in calculating the fields on the top (positive Z axis). We further assume that the field in the aperture is approximately polarized linearly.

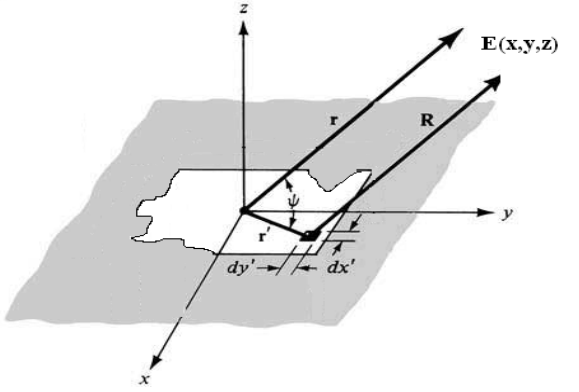

Fig.1. Radiated fields from a typical aperture.

Begin with the vector potential [22]

$$\boldsymbol{A} = \frac{1}{4\pi}\iint_S \boldsymbol{J}_s(r')\frac{e^{-jKR}}{R}ds' \tag{4}$$

Where

$$R = |\bar{r} - \bar{r}'| = \left[(x-x')^2 + (y-y')^2 + z^2\right]^{1/2} \tag{5}$$

The *H* field can be obtained by

$$\boldsymbol{H} = \nabla_r \times \boldsymbol{A} \tag{6}$$

Putting these together gives

$$\begin{aligned}\boldsymbol{H} &= \frac{1}{4\pi}\nabla_r \times \int_V \boldsymbol{J}_s(r')\frac{e^{-jKR}}{R}dv' \\ &= \frac{1}{4\pi}\int_V \nabla_r \times \left[\boldsymbol{J}_s(r')\frac{e^{-jKR}}{R}\right]dv'\end{aligned} \tag{7}$$

The integrand can be simplified by the following:

$$\begin{aligned}&\nabla_r \times \left[\boldsymbol{J}(r')\frac{e^{-jKR}}{R}\right] \\ &= \frac{e^{-jKR}}{R}\nabla_r \times \boldsymbol{J}(r') - \boldsymbol{J}(r') \times \nabla_r \frac{e^{-jKR}}{R} \\ &= -\boldsymbol{J}(r') \times \nabla_r \frac{e^{-jKR}}{R}\end{aligned} \tag{8}$$

The $\nabla_r \times \boldsymbol{J}(r')$ term can be dropped because $\boldsymbol{J}(r')$ is only a function of r'. Also,

$$\nabla_{r'}\frac{e^{-jKR}}{R} = -\nabla_r \frac{e^{-jKR}}{R} \tag{9}$$

And

$$\nabla_r \frac{e^{-jKR}}{R} = \frac{e^{-jKR}}{R}(jK + \frac{1}{R})\hat{r} \tag{10}$$

Where

$$\hat{r} = r_x\hat{x} + r_y\hat{y} + r_z\hat{z} = \frac{\boldsymbol{R}}{R} \tag{11}$$

Now we have

$$\boldsymbol{H} = \frac{1}{4\pi}\iint_V (\boldsymbol{J}(r') \times \hat{r})(jK + \frac{1}{R})\frac{e^{-jK\boldsymbol{R}}}{R}dv' \tag{12}$$

By the principle of duality, we can deduce the following equation:

$$\boldsymbol{E} = \frac{-1}{4\pi}\iint_V (\boldsymbol{M}(r') \times \hat{r})(jK + \frac{1}{R})\frac{e^{-jK\boldsymbol{R}}}{R}dv' \tag{13}$$

We know that the fields in the aperture result from an *x*-polarized plane wave, and the direction normal to the aperture. In accordance with the equivalence principle and image theory, the magnetic surface currents in the aperture are known to be twice the tangential electric fields [22].

$$\begin{aligned}\boldsymbol{M} &= 2\boldsymbol{E_a} \times \hat{n} \\ &= 2E_a\hat{x} \times \hat{z} = -2E_a\hat{y}\end{aligned} \tag{14}$$

Where the $\boldsymbol{E_a}$ is total electric field over the aperture surface. Hence,

$$\boldsymbol{E} = \frac{1}{4\pi}\iint_{aper} (2E_a(r')\hat{y} \times \hat{r})(jK + \frac{1}{R})\frac{e^{-jKR}}{R}dS' \tag{15}$$

From (11)

$$\hat{y} \times \hat{r} = (r_x\hat{z} - r_z\hat{x}) \tag{16}$$

So we can write the *E* field in terms of the two polarizations:

$$E_x = \frac{1}{2\pi}\iint_{aper} r_z.E_a(jK + \frac{1}{R})\frac{e^{-jKR}}{R}dS \tag{17}$$

$$E_z = -\frac{1}{2\pi}\iint_{aper} r_x.E_a(jK + \frac{1}{R})\frac{e^{-jKR}}{R}dS \tag{18}$$

Note that r_x and r_z represent the portions of the unit vector r' in the *x* and *z* directions, respectively. We will further separate E_x into two terms:

$$\begin{aligned}E_x &= \frac{1}{2\pi}\iint_{aper} r_z.E_a.jK\frac{e^{-jKR}}{R}dS' \\ &+ \frac{1}{2\pi}\iint_{aper} r_z.E_a\frac{e^{-jKR}}{R^2}dS'\end{aligned} \tag{19}$$

Starting with the first term, we will rewrite it as an function of *x, y* and *z*

$$E_{x1}(x,y,z) = \frac{1}{2\pi}\iint_{aper} r_z.\frac{\hat{E}_a(x',y')}{R}.jKe^{-jKR}dx'dy' \tag{20}$$

For the far-field observations *R* can most commonly be approximated by

$$\begin{aligned}R &\approx r - r'\cos\psi && \text{for phase variation,} \\ R &\approx r && \text{for amplitude variation,}\end{aligned} \tag{21}$$

Where ψ is the angle between the vectors r and r'. The term $r'\cos\psi$ can be written by [23]

$$r'\cos\psi = x'\sin\theta\cos\phi + y'\sin\theta\sin\phi \quad (22)$$

So, we can write (20) as

$$E_{x1}(x,y,z) = j\frac{Ke^{-jKr}}{2\pi\, r}\iint_{aper} r_z.\hat{E}_a(x',y') .e^{jK(x'\sin\theta\cos\phi+y'\sin\theta\sin\phi)}dx'dy' \quad (23)$$

Similarly for the second term of (19)

$$E_{x2}(x,y,z) = \frac{e^{-jKr}}{2\pi\, r^2}\iint_{aper} r_z.\hat{E}_a(x',y') .e^{jK(x'\sin\theta\cos\phi+y'\sin\theta\sin\phi)}dx'dy' \quad (24)$$

The total E_x field is the sum of the two terms in (23) and (24), so (19) now can be written as

$$E_x(x,y,z) = (jK+\frac{1}{r})\frac{e^{-jKr}}{2\pi\, r}\iint_{aper} r_z.\hat{E}_a(x',y') .e^{jK(x'\sin\theta\cos\phi+y'\sin\theta\sin\phi)}dx'dy' \quad (25)$$

Obviously, we would obtain identical expressions for the calculation of E_z (18), except with a r_x term instead of a term r_z. Thus

$$E_z(x,y,z) = (jK+\frac{1}{r})\frac{e^{-jKr}}{2\pi\, r}\iint_{aper} r_x.\hat{E}_a(x',y') .e^{jK(x'\sin\theta\cos\phi+y'\sin\theta\sin\phi)}dx'dy' \quad (26)$$

The radiated field, as given by (25) and (26), involves the integration over the entire domain of the problem. In two dimensional problems, the conventionally used quadrature rules is time consuming. This integration cannot be performed analytically or numerically by quadrature rules and approximate methods have to be developed. This essentially makes the FEM solution an approximate one. The function in the integrand is usually modified and approximated before performing the integration. The technique adopted here is the MCI technique that does not require the integrand function to be modified. Rather, the singularity problem is removed due to the characteristic property of the MCI for example the integration based on random number generation.

For two dimensional integration, the number of the evaluations of the integrand performed using the quadrature methods is of the order of M^2 where M is the number of intervals into which the *x* and *y* axes are divided. On the other hand, the number of the evaluations required in MCI is of the order of N, where N is the total number of uniformly random distributed points generated over the entire domain, independent of the dimensionality [24]. For this purpose the image processing technique is utilized. So that the image of the radiation surface in Mono Color BMP format, with the largest dimensions of the plane along the *x* and *y* directions, is considered. By this idea, each pixel of the image represents a specific location of the surface of the aperture radiator. The surface can be sampled by the random selection of the image pixels. It is shown in this paper that the MCI applied for the evaluation of radiation gives results which are in good agreement with those obtained from Gaussian quadrature rules and FEM analysis.

4. VERIFICATION OF THE MCI TECHNIQUE ON VARIOUS APERTURES

Simulations are performed for the formulation of the aperture radiation using the MCI technique for various apertures. Each of the apertures, in both cases of uniform and TE_{10}/TE_{11}/TE_{c10}-modes distributions has been studied. A 3D full-wave FE electromagnetic field simulator (HFSS v.13) [25] is used for the mode distributions. To validate the radiation problem and the implementation of the MCI in the solution of the electric fields, the two- and three-dimensional patterns of the far-zone fields radiated by the apertures have been plotted. In many applications, however, only a pair of two-dimensional plots is usually sufficient. These are the principal *E*- and *H*-plane patterns. The *E*-plane pattern is on the *y*-*z* plane ($\varphi = \pi/2$) and the *H*-plane is on the *x*-*z* plane ($\varphi = 0$). In addition, in order to ensure the accuracy of the results, the fields calculated by the proposed technique in this paper, are plotted and compared with that of the conventional theoretical and quadrature results, with respect to the elevation angle in *y*-*z* and *x*-*z* planes respectively.

4.1 Rectangular Aperture

In the first case, a rectangular aperture with uniform distribution on infinite ground plane is considered with the dimensions of a=2λ and b=3λ, where λ is the wavelength. The schematic of this aperture is shown in Fig. 2. The tangential E field over aperture is given by:

$$\boldsymbol{E}_a = \hat{\boldsymbol{a}}_y E_0 \qquad \begin{matrix} -\frac{a}{2} \le x' \le \frac{a}{2} \\ -\frac{b}{2} \le y' \le \frac{b}{2} \end{matrix} \quad (27)$$

The results in Figs. 3(a) and 3(b) show the two-dimensional *E*- and *H*-plane patterns, for three different numbers N of random points taken for the MCI. These figures make two points evident. First, the results for all the values of N show a good agreement with the results obtained by Balanis [23] using the radiation integral equations (theoretical). Second, the evaluation

of the radiated fields by the proposed MCI technique is in good agreement with the conventional two-dimensional quadrature rule with M=30 points.

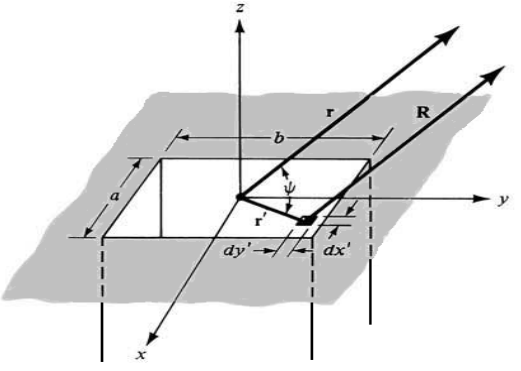

Fig. 2. Rectangular aperture on an infinite electric ground plane.

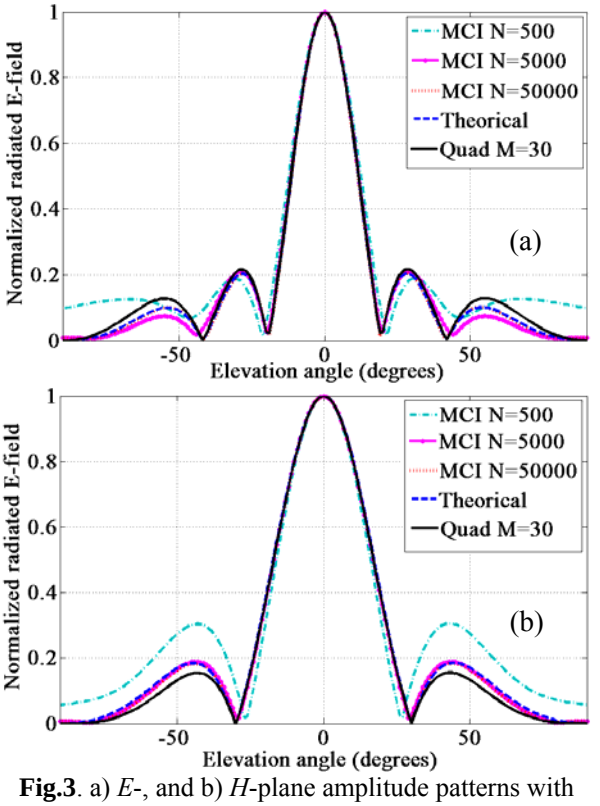

Fig.3. a) *E*-, and b) *H*-plane amplitude patterns with a=2λ and b=3λ.

Nevertheless it is important to state that how many N points are sufficient in the MCI for the problem under investigation, thereby decreasing the computational burden. For this purpose, the Fig. 3(a) for different values of N from 500 to 50,000, with step size 500, has been plotted again and studied. Fig. 4 shows the error percentage of the changes per Ns than the theoretical result. As it is clear from this figure, for N=17000 and more there are the errors around 1% and even less. Thus this number of random points is enough for this kind of problem. This analysis and the obtained N=17000 are independent of zone size and shape of the aperture.

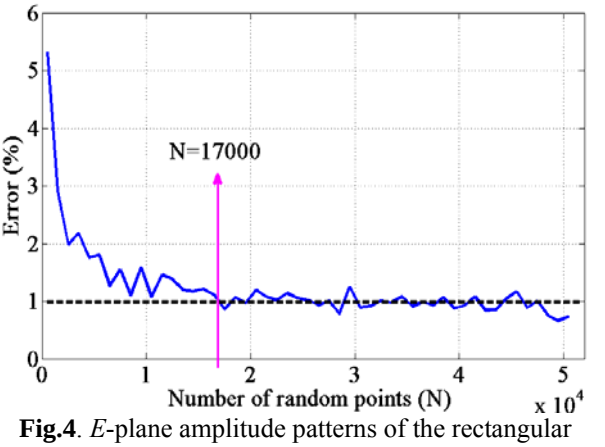

Fig.4. *E*-plane amplitude patterns of the rectangular aperture on the metal plane with different values of N and error percentage of the above compared with theoretical result.

The performance of the MCI technique for the various sizes of rectangular aperture compared with Gaussian quadrature rule is shown in Table 1. The radiation integrals are done with a 30/700/25000-points Gaussian quadrature integration formula for cases 1 to 3 in Table 1, respectively. However, the same integrals only are solved with N=17000 points by Monte Carlo method for these cases. The running time increases with larger dimensions for quadrature rules, while it is constant for every size of the aperture in the MCI. Both methods are implemented on the same PC with 2.8GHz Dual Core CPU and 2GB memory.

Table1. The running time of MCI compared with Gaussian quadratre rule

Dimensions	Quad	MCI
a=2λ, b=3λ	15.43 sec	1.46 sec
a=10λ, b=15λ	170.25 sec	1.46 sec
a=50λ, b=75λ	11586.54 sec	1.46 sec

Fig. 5 shows the results for the three-dimensional field pattern. Total number of the random points for the MCI to evaluate the three-dimensional field pattern has been taken to be 17000. It is found that the results show good agreement with those obtained in [23].

In practice, a commonly used aperture is that of a rectangular waveguide mounted on an infinite ground plane. At the opening, the field is usually approximated by the dominant TE_{10}-mode. Thus

$$\boldsymbol{E}_a = \hat{\boldsymbol{a}}_y E_0 Cos(\frac{\pi}{a}x') \quad -\frac{a}{2} \le x' \le \frac{a}{2} \tag{28}$$

$$-\frac{b}{2} \le y' \le \frac{b}{2}$$

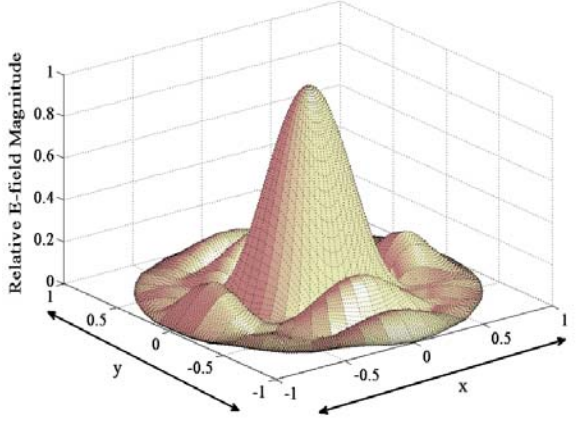

Fig. 5. Three-dimensional field pattern of a constant field with a=2λ and b=3λ.

The rectangular aperture is considered with *f*=15GHz, a=7.5mm and b=15mm, which corresponds to the 0.375 and 0.75 wavelength, respectively. Due to the limitations of PC system, FE simulation is not possible for higher wavelength. The magnitude electric distribution for this case is plotted in Fig. 6.

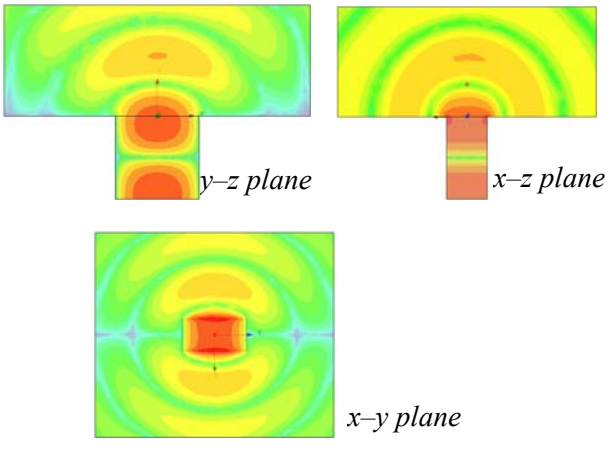

Fig.6. The electric field components maximum value envelopes at 15GHz for a rectangular aperture. This shows a TE_{10} field.

The simulated far field with the MCI in this paper is plotted and compared with that of the FE simulation, with respect to the elevation angle in *x*-*z* and *y*-*z* planes respectively. The results are plotted in Figs. 7(a) and 7(b) for this case. The running times of MCI and FE simulations are 1.46sec and 956sec, respectively.

4.2 Circular Aperture

In the second case, a circular aperture with uniform distribution of a=1.5λ is considered, as shown in Fig. 8. The field over the aperture is assumed to be constant as:

$$\boldsymbol{E}_a = \hat{\boldsymbol{a}}_y E_0 \qquad \rho' \le a \tag{29}$$

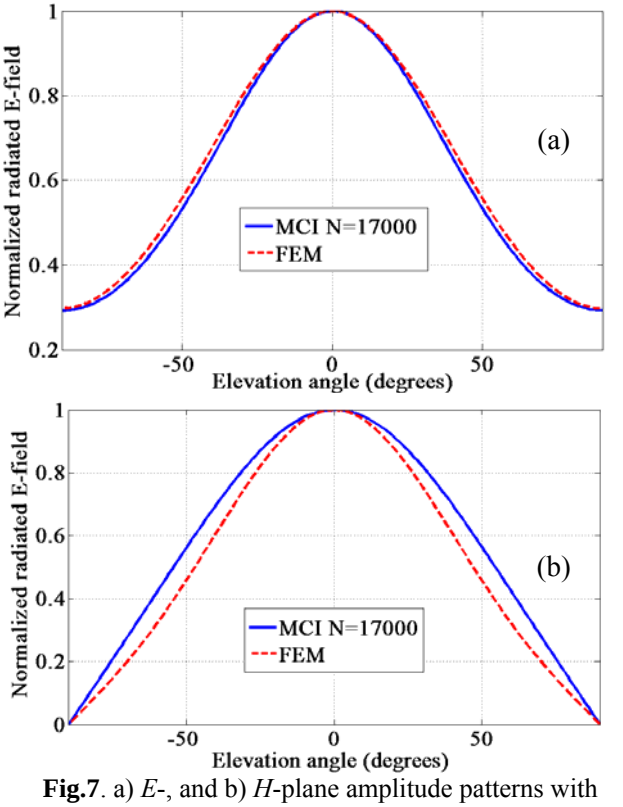

Fig.7. a) *E*-, and b) *H*-plane amplitude patterns with a=0.375λ and b=0.75λ.

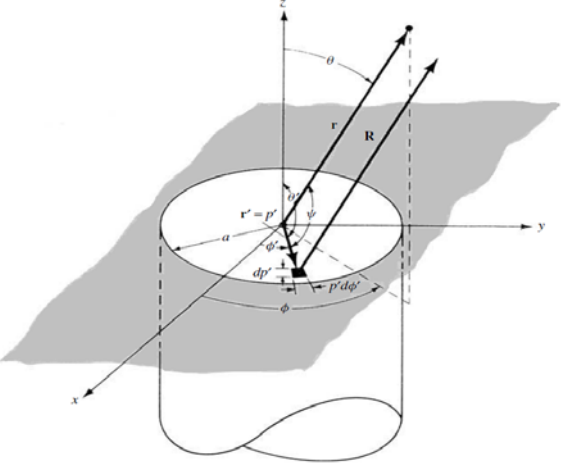

Fig.8. Circular aperture mounted on an infinite ground plane.

Fig. 9(a) shows the two-dimensional pattern of the far-zone fields radiated by aperture versus elevation angle (θ) in both of *x*-*z* and *y*-*z* planes. Total number of the random points for the MCI to assess the field

patterns has been taken to be N=17000. The three-dimensional radiation pattern of the aperture as the function of θ and φ is shown in Fig. 9(b).

A very practical antenna is a circular waveguide of the radius a mounted on an infinite ground plane. The field distribution over the aperture is usually that of the dominant TE_{11}-mode for a circular waveguide given by:

$$\boldsymbol{E}_a = \hat{\boldsymbol{a}}_\rho E_\rho + \hat{\boldsymbol{a}}_\varphi E_\varphi$$

$$E_\rho = \frac{E_0}{\rho'} J_1\left(\frac{x'_{11}}{a}\rho'\right)\sin\phi' \qquad x'_{11} = 1.841 \quad \rho' \le a \qquad (30)$$

$$E_\varphi = E_0 \frac{\partial}{\partial \rho'}\left[J_1\left(\frac{x'_{11}}{a}\rho'\right)\right]\cos\phi'$$

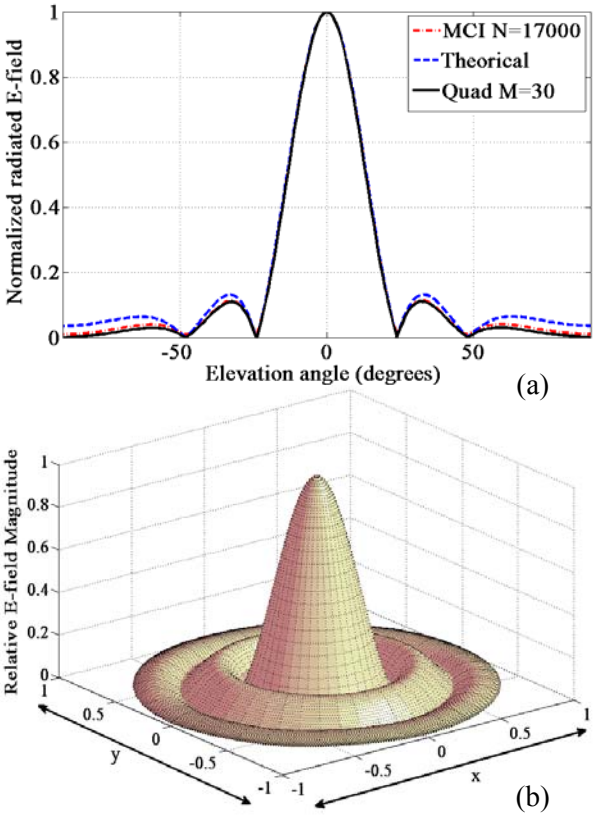

Fig.9. a) *E*-, *H*-plane amplitude patterns and b) Three-dimensional field pattern of a constant field with a=1.5λ.

In this case *f*=15GHz and a=7.5mm. Fig. 10 shows the distribution of the electric field magnitude entire surfaces. Figs. 11(a) and 11(b) show the simulated MCI and FE versus elevation angle in *x*-*z* and *y*-*z* planes, respectively. The results shown in Table 2 compare running times of these methods for various dimensions of the aperture radius.

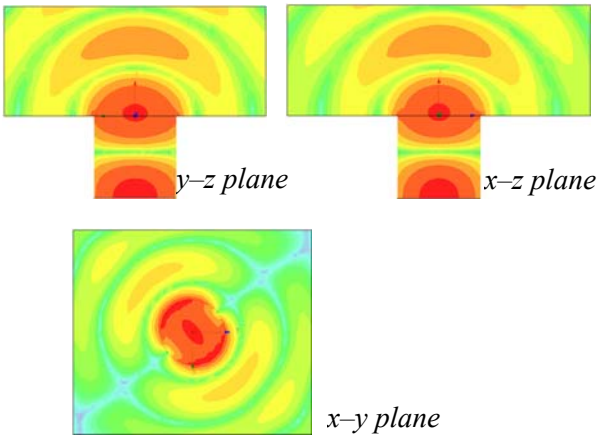

Fig.10. The electric field components maximum value envelopes at 15GHz for a circular aperture. This shows a TE_{11} field.

Table2. The running time of the MCI compared with the FEM for circular aperture

Dimensions	FE	MCI
a=7.5mm	1042.4 sec	1.65 sec
a=12mm	3564.2 sec	1.65 sec
a=18mm	5286.5 sec	1.65 sec

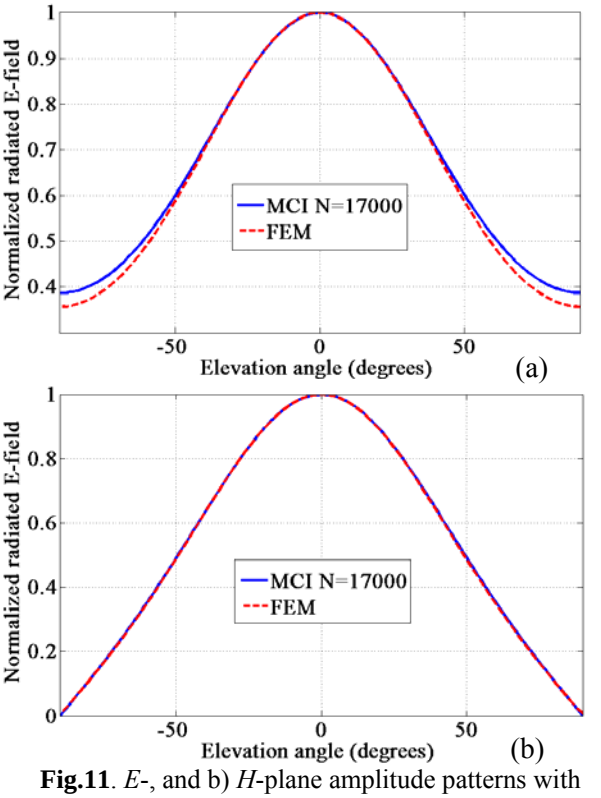

Fig.11. *E*-, and b) *H*-plane amplitude patterns with a=0.375λ.

4.3 Elliptical Aperture

In the third and final case, an elliptical aperture of a=6λ and b=2λ has been investigated with uniform distribution, as shown in Fig. 12. The coordinate system in this figure is based on elliptical-cylindrical [26]. The field distribution at the aperture is defined as [27]:

$$\boldsymbol{E}_a = \hat{\boldsymbol{a}}_y E_0 \qquad \xi' \le \cosh^{-1}\left(\frac{a}{\sqrt{a^2-b^2}}\right) \tag{31}$$

The two-dimensional patterns versus elevation angle in *E*- and *H*-planes respectively are plotted in Figs. 13(a) and 13(b). The three-dimensional pattern for the aperture is also shown in Fig. 13(c). Theoretical result has been extracted from [28-29] for this case.

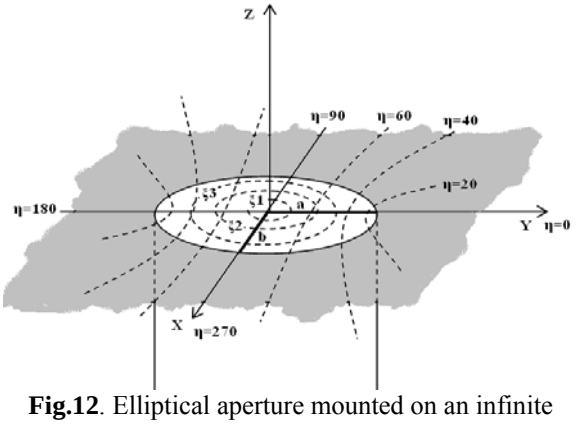

Fig.12. Elliptical aperture mounted on an infinite ground plane.

In practical apertures with elliptical cross- sections are possible candidates as feed for shaped reflectors suitable for satellite antennas giving a shaped beam. Fundamental mode in this aperture is TE_{c11}, which c indicates that the mode is even for example the Mathieu function, $T(\xi,\eta)$ are solved. The field distribution is given by [27]:

$$\boldsymbol{E}_a = \hat{\boldsymbol{a}}_\xi E_\xi + \hat{\boldsymbol{a}}_\eta E_\eta$$

$$E_\xi = \frac{-E_0}{\sqrt{\cosh(2\xi')-\cos(2\eta')}}\frac{\partial}{\partial\eta'}T(\xi',\eta') \tag{32}$$

$$E_\eta = \frac{E_0}{\sqrt{\cosh(2\xi')-\cos(2\eta')}}\frac{\partial}{\partial\xi'}T(\xi',\eta')$$

An elliptical waveguide terminate in an infinite ground plane in which *f*=10GHz, a=7.5mm, and b=3.75mm, is considered. Fig. 14 shows the magnitude of the electric field in the surface. Figs. 15(a) and 15(b) show the comparison between the FE and MCI simulated in the *E*- and *H*-plane, respectively. In the Table 3 run-time of the two methods are shown.

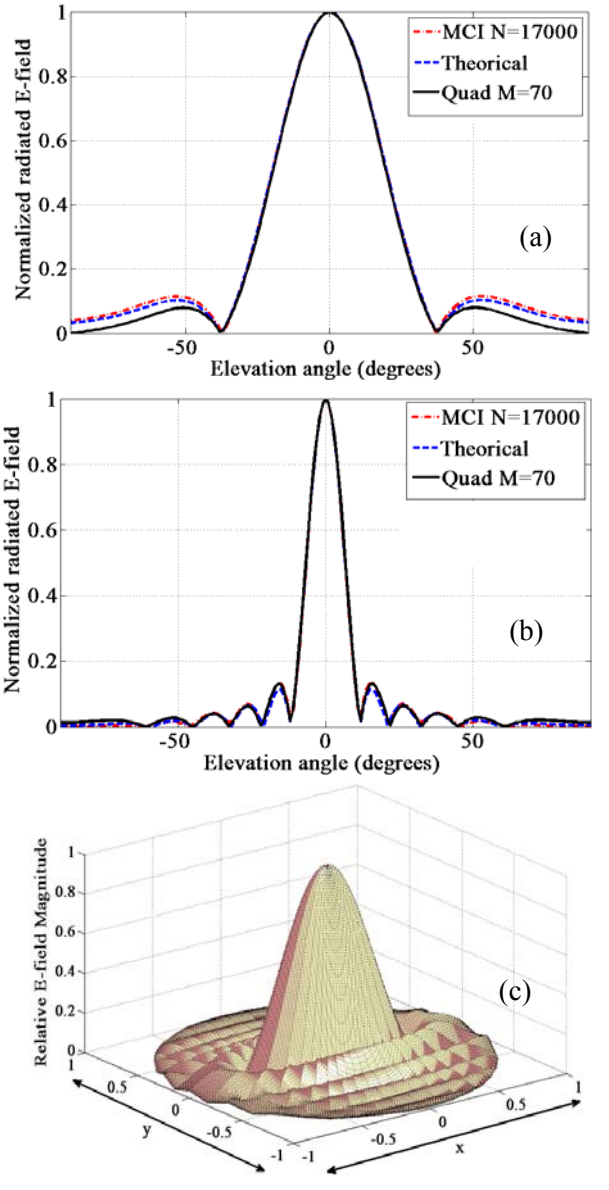

Fig. 13. a) *E*-, b) *H*-plane amplitude patterns and c) Three-dimensional field pattern of a constant field.

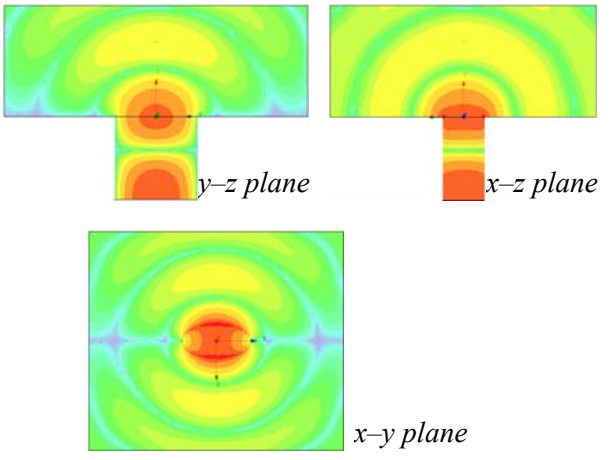

Fig.14. The electric field components maximum value envelopes at the 15GHz for an elliptical aperture. This shows a TE_{c11} field.

It is clear from Fig. 7 through Fig. 15 that calculated fields by the proposed MCI technique and FE implementation in evaluation of the radiation fields, is in good agreement with the theoretical and quadrature results.

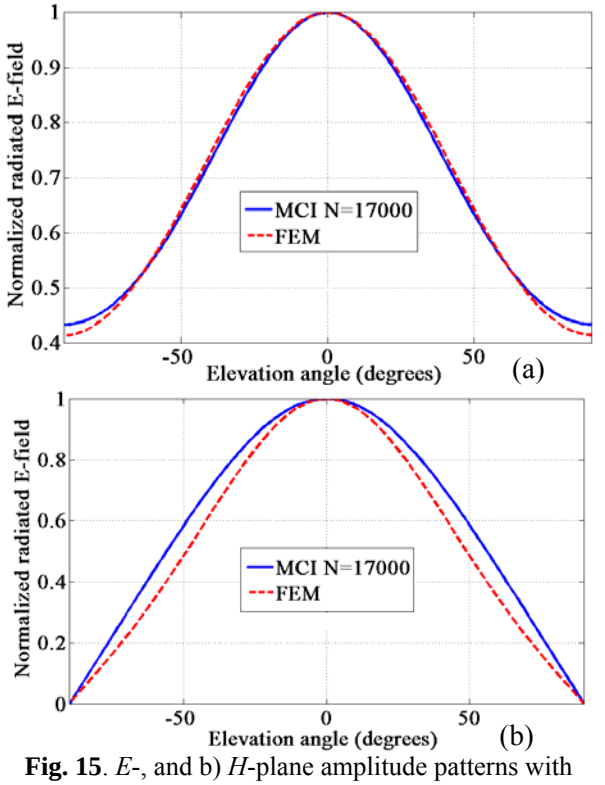

Fig. 15. *E*-, and b) *H*-plane amplitude patterns with a=0.0.375λ and b=0.1875λ.

Table 3. The running time of MCI compared with FEM for elliptical aperture

Dimensions	FE	MCI
a=7.5mm, b=3.75mm	1858.2 sec	2.13 sec
a=10mm, b=5mm	3385.5 sec	2.13 sec
a=15mm, b=7.5mm	6582.7 sec	2.13 sec

5. CONCLUSION

In this paper, a new technique based on the Monte Carlo integration is proposed to solve the problem of the far-field integral equation from apertures. This technique is capable of reducing the computational burden and running time in the integral equation compared to the FEM and Gaussian qudrature rule. Especially in the case of two and higher dimensional problems, the MCI technique is superior to the conventional quadrature methods for integration. This is because of the fact that this technique is independent of the dimensions of the problem, involving only uniform generation of the random points inside the domain of the integration. In addition to this, the rapid convergence of the MCI with respect to the total number of the random points, the small number of the functions is needed to provide accurate results. To verify the technique, it is applied to the problem of the radiation from rectangular, circular and elliptical apertures. The two and three-dimensional radiation patterns over the apertures have been evaluated and plotted. Since comparisons are available, it is found that this technique yields the results comparable very closely to the those of the other numerical integration methods.

3. ACKNOWLEDGMENT

This research was supported by Semnan University. Also, the authors would like to thank the Office of Brilliant Talents at the Semnan University for financial support.

REFERENCES

[1] Kozakoff. D. J, **"Analysis of Radome Enclosed Antennas, 2nd edition, Artech House, Norwood, MA",** 2009.

[2] Van Bladel J. G, **"Electromagnetic Fields, 2nd Edition",** *John Wiley & Sons*, 2007.

[3] Balanis. C. A, **"Advanced Engineering Electromagnetics, 2nd Edition",** Wiley, New York, 2012.

[4] Orfanidis. S. J, **"Electromagnetic Waves and Antennas"**, *Rutgers University*, 2008.

[5] Volakis. J. L, Chatterjee. A, and Kempel. L. C, **Finite Element Method Electromagnetics: Antennas",** *Microwave Circuits, and Scattering Applications, Wiley,* New York, 1998.

[6] JinJ. M, **The Finite Element Method in Electromagnetics, 2nd Edition, Wiley,** 2002.

[7] Gibson. W. C, **The Method of Moments in Electromagnetics, CRC Press Inc**, 2008.

[8] Taflove. A and Hagness. S. C, **Computational Electromagnetic: The Finite-Difference Time-Domain Method,** *Artech House, Boston, UK*, 2005.

[9] Vrancken. M, Schols. Y, Aerts. W, and Vandenbosch. G. A. E, "**Benchmark of full Maxwell 3-dimensional electromagnetic field solvers on prototype cavity-backed aperture antenna,**" *AEU– Int. J. Electron. Commun.*, Vol. 61, pp. 363–369, 2007.

[10] Fakharian. M. M, and Rezaei. P, "**Parametric study of UC-PBG structure in terms of simultaneous AMC and EBG properties and its applications in proximity-coupled fractal patch antenna,**" *Int. J. Eng., Trans. A: Basics*, BVol. 25, pp. 389–396, 2012.

[11] Leung. K. W, and LamH. Y, "**Aperture antennas on probe-fed hemispherical metallic cavities,**" *IEEE Trans. Antennas Propagat.*, Vol. 54, pp. 3556–3561, 2006.

[12] Rolland. A, Ettorre. M, Drissi. M, Coq. L. Le, and Sauleau. R, "**Optimization of reduced-size smooth-walled conical horns using BoR-FDTD and genetic algorithm,**" *IEEE Trans. Antennas Propagat.*, Vol. 58, pp. 3094–3100, 2010,

[13] Sadiku. M. N. O, **Monte Carlo Methods for Electromagnetics, CRC Press Inc,** New York, 2009.

[14] Dedrick. K. G, Hessing. A. R, and Johnson. G. L, "**Bistatic radar scattering by randomly oriented wires,**" *IEEE Trans. Antennas Propagat.*, Vol. 26, pp. 420–426, 1978.

[15] Barrowes. B. E, Ao. C. O, Teixeira. F. L, Kong. J. A, and Tsang. L, "**Monte Carlo simulation of electromagnetic wave propagation in dense random media with dielectric spheroids,**" *IEICE Trans. Electron.*, Vol. 83, pp. 1797–1802, 2000.

[16] K. Sarabandi. K, "**Monte Carol simulation of scattering from a layer of vertical cylinders,**" *IEEE Trans. Antennas Propagat.*, Vol. 41, pp. 465–475, 1993.

[17] Mishra. M and Gupta. N, "**Monte Carlo Integration Technique for the Analysis of Electromagnetic Scattering from Conducting Surfaces,**" *Prog. Electromag. Res.*, Vol. 79, pp. 91–106, 2008.

[18] Mishra. M, and Gupta. N, "**Quasi Monte Carlo integration technique for method of moments solution of EFIE in radiation problems,**" *Appl. Comput. Electromag. Soci. J.*, Vol. 24, pp. 306–311, 2009.

[19] Mishra. M, and Gupta. N, "**Singularity treatment for integral equations in electromagnetic scattering using Monte Carlo integration technique,**" *Microwave Opt. Tech. Lett.*, Vol. 50, pp. 1619–1623, 2008.

[20] Owen. A. B, **Monte Carlo and Quasi-Monte Carlo Methods 2010**, *Springer Proceedings in Mathematics & Statistics*, 2012.

[21] Ulaby. F. T, **Fundamentals of applied electromagnetics,** *Pearson/Prentice Hall,* 2007.

[22] Stutzman. W. L, and Thiele. G. A, **Antenna Theory and Design, 2nd Edition,** New York: Wiley, 1997.

[23] Balanis. C. A, **Antenna Theory Analysis and Design, Wiley**, New York, 2005.

[24] Gentle. J. E, **Random Number Generation and Monte Carlo Methods, Springer**, 2003.

[25] Ansoft High Frequency Structure Simulator (HFSS). ver. 13, Ansoft Corporation, Canonsburg, PA, 2010.

[26] Fouche. C, "**Elliptical applicator design through analysis, modeling and material property knowledge,**" M.Sc. Thesis, University of Stellenbosch, 2006.

[27] Bornemann. J, "**waveguide technology,**" http://www.ece.uvic.ca/~jbornema/ELEC524/524-03-WgTech.pdf

[28] Kathuria. Y, "**Radiation patterns of an elliptical aperture in the Fresnel region,**" *IEEE Trans. Antennas Propagat.*, Vol. 33, pp. 572–575, May 1985.

[29] Kathuria. Y, "**Far-field radiation patterns of elliptical apertures and its annulli,**" *IEEE Trans. Antennas Propagat.*, Vol. 31, pp. 360–364, 1983.